

Gravitational radiation from spinning-black-hole binaries: The orbital hang up

M. Campanelli, C. O. Lousto, and Y. Zlochower

Department of Physics and Astronomy, and Center for Gravitational Wave Astronomy,
The University of Texas at Brownsville, Brownsville, Texas 78520

(Dated: February 20, 2019)

We study the dynamics of spinning-black-hole binaries by numerically solving the full nonlinear field equations of General Relativity. We compute trajectories, merger times, and radiation waveforms. We find that the last stages of the orbital motion of black-hole binaries are profoundly affected by the individual spins. In order to cleanly display its effects, we consider two equal-mass holes with individual spin parameters $S/m^2 = 0.75$, both aligned and anti-aligned with the orbital angular momentum. We choose initial data corresponding to quasicircular orbits with a period of $125M$ for both cases. The computed merger time for the aligned spin case is $225M$, performing nearly three orbits before merger, while for the anti-aligned case the merger time is $105M$, performing just less than one orbit before merger. The total energy radiated for the former case is 6% while for the latter it is only 2% . The final Kerr hole remnants have rotation parameters $a/M = 0.9$ and $a/M = 0.44$ respectively, showing the difficulty of creating a maximally rotating black hole out of the merger of two spinning holes.

PACS numbers: 04.25.Dm, 04.25.Nx, 04.30.Db, 04.70.Bw

I. INTRODUCTION

Spinning black holes play an important role in some of the most energetic astrophysical phenomena in the universe. They form part of the main engine of gamma-ray bursts, being much more efficient at converting matter into radiation than non-spinning black holes. They are also responsible for the radio jets observed in active galactic nuclei, and the merger of two non-aligned spinning black holes is the likely explanation for the rapid directional changes observed in these jets when galaxies collide [1]. Recent estimates [2] of the spin of stellar mass black holes by spectral fitting of the X-Ray continuum set the rotation parameter of two dynamically formed black holes at $a/M \approx 0.75$. Accretion, of course, can spin up black holes, reaching up to a sub-maximal spin rate of $a/M \approx 0.95$, when magneto-hydrodynamics is taken into account [3, 4]. Other models using the combined effects of gas accretion and binary-black-hole coalescence suggest that black holes may be rapidly rotating in all epochs [5].

The first simulations of orbiting black-hole binaries were reported in Ref. [6] and verified in Ref. [7]; however, these did not allow for gravitational wave extraction. During this past year new numerical techniques to solve the field equations of General Relativity have been developed [8, 9, 10] that make it possible to stably evolve black-hole binaries for several orbits and to compute the corresponding gravitational waveforms [11, 12, 13]. Numerical simulations of unequal-mass black-hole binaries, along with the calculation of the merger kicks, have been reported in Refs [14, 15, 16]. While research has been mainly focused on initially non-spinning black holes, there are important questions to be addressed when we consider highly-spinning black holes. Prominent among these questions are the dependence of the total radi-

ated energy and angular and linear momentum on the magnitude and orientation of the spins of the individual black holes in the binary system, as well as whether the radiated waveform becomes more complex in the spinning case. (The waveforms computed for the last few orbits of non-spinning-black-hole binaries in nearly quasicircular orbits appears particularly simple and universal [11, 12, 17].)

In this paper we study how the emission of gravitational radiation affects the orbital trajectory of highly-spinning, equal-mass black holes as a function of the spin orientation. In order to maximize the effect, we consider black-hole binaries with both spins aligned and anti-aligned with the orbital angular momentum. We shall consider quasicircular orbit initial data with the same initial orbital period (as determined by the third post-Newtonian expansion). In this way differences in the subsequent evolution can be attributed to the differences in the generation and emission of gravitational radiation.

Our choice of initial data is that of the Bowen [18] type in the puncture implementation [19] (without excision of the interior of the holes). These data families have been used to determine the innermost stable circular orbit (ISCO) for different values of the black hole spins in a binary, aligned and anti-aligned with the orbital angular momentum [20], generalizing the effective potential method used for non-spinning holes. Due to the repulsive nature of the spin-orbit interaction, the $++$ cases (spins aligned with the orbital momentum) produce ISCOs at closer orbital separations than in the non-spinning case. The $--$ cases (spins counter-aligned with the orbital momentum) have an effective attractive interaction and hence produce ISCO locations at larger orbital separations.

In Ref. [21] the numerical evolutions of these ISCO

TABLE I: Initial data for quasicircular orbits of black-hole binaries with spin. The holes have proper horizon separation l , with puncture locations $(0; y; 0)$, linear momenta $(P; 0; 0)$, and spin $(0; 0; S)$. J is the total angular momentum, L is the orbital angular momentum, M is the orbital frequency, m is the individual puncture mass, and E_b is the binding energy. All in units of the ADM mass M .

$S=m^2$	$+0.75$	-0.75
$l=M$	9.2679	10.3441
$y=M$	3.0595	3.465
$P=M$	0.1291	0.1382
$S=M^2$	$+0.1939$	-0.1924
$J=M^2$	1.178	0.573
$L=M^2$	0.790	0.958
M	0.0500	0.0500
$m=M$	0.335	0.335
$E_b=M$	-0.170	-0.130

configurations were studied for relatively modest values of the spins ($0.25 \leq S=m^2 \leq 0.17$, m being the horizon mass of the individual holes) using the ‘Lazarus’ technique of matching full numerical evolutions to perturbation theory. In those evolutions the spin of the remnant Kerr hole increased with $S=M^2$ for the aligned case. Extrapolation to maximally spinning individual holes indicated that the remnant would remain sub-maximal for $S=m^2 < 0.85$. We will revisit this scenario, now reaching much higher values of the individual spins in order to make a more accurate statement.

II. INITIAL DATA

We use the Brandt-Brugmann puncture approach along with the elliptic solver BAM_Elliptic [19, 22] to compute initial data. Table I gives our choice of initial parameters. We have taken a fiducial angular frequency of $M = 0.05$, which corresponds to an orbital period of approximately $T = 125M$, as in our previous simulation for non-spinning black holes [11] (where the binary completed more than a full orbit before the black holes merged). We choose individual spins $S = 0.75m^2$ to guarantee that the total angular momentum in the aligned case exceeds M^2 , the theoretical maximum allowed value for a common horizon to form. The gravitational radiation emitted should efficiently carry out angular momentum from the system in order for the cosmic censorship conjecture to hold [23]. We can thus begin to explore its validity here, and this will be the subject of a more detailed study in a forthcoming paper by the authors.

With our choices of the spin and the orbital angular frequency, we determine the remaining orbital parameters by imposing quasicircular orbits according to the second post-Newtonian expansion of spinning particles [24] extended by the third-order orbital corrections [25]. We then give those parameters to the exact Bowen solution of the momentum constraints and solve for the conformal

factor of the (conformally flat) three-metric to complete our choice of the initial data. We have also briefly studied the effects of a different choice of the form of the initial data (Kerr conformal extrinsic curvature) for spinning black holes, as proposed in Ref. [26], and we will report the results in a forthcoming paper.

The choice of the orbital frequency $M = 0.05$ ensures that the black-hole binaries start well outside the ISCO, as can be inferred by extrapolation of the results of Ref. [20] to $S=m^2 = 0.75$ (see also Table I of Ref. [21]).

III. TECHNIQUES

We evolved these black-hole-binary data sets using the `LazEv` [27] implementation of the moving puncture approach [9, 10]. In our version of the moving puncture approach [9] we replace the BSSN [28, 29, 30] conformal exponent χ , which is infinite on the punctures, with the C^4 field $\chi = \exp(-\chi^4)$. This new variable, along with the other BSSN variables, will remain finite provided that one uses a suitable choice for the gauge (see [10] for an alternative approach to moving punctures).

We obtained accurate, convergent waveforms by evolving this system in conjunction with a modified 1+log lapse, a modified Gamma-driver shift condition [9, 31], and an initial lapse α_{BL}^4 . The lapse and shift are evolved with

$$(\partial_t - \mathcal{L}_\beta) \alpha = -2K; \quad (1)$$

$$\partial_t \beta^a = \beta^a; \quad \partial_t \beta^a = 3\alpha \partial_t \tilde{\beta}^a - \beta^a; \quad (2)$$

These gauge conditions require careful treatment of near the puncture in order for the system to remain stable [9, 11]. For our version of the moving puncture approach, we find that the product $\tilde{A}^{ij} \partial_j$ has to be C^2 on the puncture. In the spinning case, \tilde{A}^{ij} is $O(r)$ on the puncture, thus requiring that ∂_j / r^3 to maintain differentiability. We therefore choose an initial lapse α_{BL}^4 (which is $O(r^4)$ and C^4 on the puncture). In particular, $(\partial_t - \mathcal{L}_\beta) \alpha = -2(1 + \frac{4}{\alpha_{BL}^4})$ reproduces the isotropic Schwarzschild lapse at large distances from the hole. The initial values of $\tilde{\beta}^i$ and β^i were set to zero.

The minimum resolution required to accurately model the dynamics of the merger scales with m . We expect satisfactory results for a minimum resolution of $h = M/30$ (based on the non-spinning case, where satisfactory results were obtained with $h = M/21$, and the ratio of the puncture masses in the spinning and non-spinning cases), M being the total ADM mass.

We exploited the P -rotational symmetry about the z -axis as well as the reflection symmetry about the xy plane to reduce the size of the computational domain by one quarter.

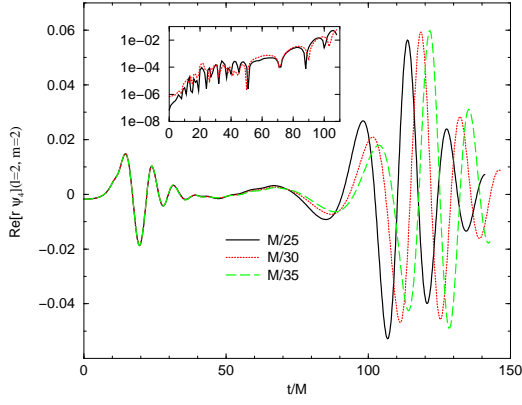


FIG. 1: The real ($\ell = 2; m = 2$) component of the r_4 in the Quasi-Kinnersley tetrad at $r = 10M$ for the -0.75 case. The inset shows the differences $r_4(M=25) - r_4(M=30)$ (solid line) and $r_4(M=30) - r_4(M=35)$ (dotted line), the latter rescaled by 2^{33} to demonstrate fourth-order convergence. The lack of convergence for $t < 20M$ is due to round-off effects in the initial data solver.

IV. RESULTS

We evolved the -0.75 configuration using grid sizes of 320^2 , 640 , 384^2 , 768 , and 448^2 , 896 and resolutions of $M=25$, $M=30$, and $M=35$ respectively. We used a multiple transition scheme [11] to push the physical boundaries to $134M$. We calculate r_4 in the Quasi-Kinnersley frame using the recently developed techniques of Ref. [32] that allow a meaningful extraction closer to the hole. In Fig. 1 we show the real part of the ($\ell = 2; m = 2$) mode of r_4 for the -0.75 case (extracted at $r = 10M$) for these resolutions, as well as a convergence plot of these data. The waveforms show fourth-order convergence up to $t = 110M$. The phase error from the $h = M = 25$ run becomes too large to measure a meaningful convergence rate after $t = 110M$. Higher resolution runs will remain convergent, as demonstrated by the better phase agreement between the $M = 30$ and $M = 35$ runs. The lack of convergence for $t < 20M$ appears to be due to round-off effects in the initial data solver. We extract the waveform at $10M$ to minimize the effects of the extreme scheme deresolution (and boundary effects). The radiated energy and angular momentum calculated at $r = 15M$ were $(2.1 \pm 0.2)\%$ and $(1.9 \pm 0.2)\%$ respectively.

We used Jonathan Thornburg's AHFinderDirect [33] to calculate the apparent horizons. We find that the common horizon is first detected at $t = 105.5M$ and has a mass of $0.979 \pm 0.01M$ and rotation parameter of $a = M_H = 0.44 \pm 0.01$ (where M_H is the horizon mass of the remnant Kerr hole). During the merger 2.1% of the mass and $(26 \pm 2)\%$ of the angular momentum are converted into radiation. Note that the waveforms have been truncated (due to a non-ideal choice for the gauge) and the estimates for the radiated energy angular momentum from the waveform are less accurate. However,

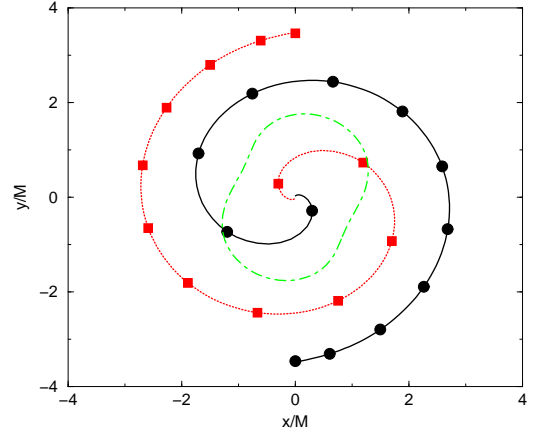


FIG. 2: The puncture trajectories on the xy plane for the -0.75 case with resolution $M = 35$. The spirals are the puncture trajectories with ticks every $10M$ of evolution. The dot-dash 'peanut shaped' figure is the first detected common horizon at $105.5M$. The period of the last orbit is around $120M$.

the estimates based on the final horizon mass remain accurate.

Figure 2 shows the trajectories of the punctures for the -0.75 configuration as well as the projection of the first common horizon on the xy plane. It is evident from the waveform and the track that the binary undergoes ~ 0.9 orbits before merging.

We evolved the $+0.75$ configuration with a grid size of 384^2 , 768 and resolution of $M = 30$. We used multiple transition scheme to push the boundaries to $159M$. In Fig. 3 we show the ($\ell = 2; m = 2$) mode of r_4 in the Quasi-Kinnersley frame for the $+0.75$ case, again extracted at $r = 10M$. Note the 'plunge' waveform is delayed by $\sim 120M$ compared to the -0.75 case. The waveform shows approximately six periods of orbital radiation prior to the plunge waveform, indicating that the binary completed approximately three orbits.

In the $+0.75$ case the first common horizon was detected at $t = 224.5M$. In this case the final horizon had a mass of $0.94 \pm 0.01M$ and spin of 0.899 ± 0.02 (indicating that $(6 \pm 1\%)$ of the mass and $(32.5 \pm 1.5)\%$ of the angular momentum are radiated away). These horizon parameters are affected by boundary errors (the horizon formed $60M$ after boundaries errors first began affecting the interior region), and runs with significantly larger grid sizes will be needed to remove this source of error. The radiated mass and angular momentum calculated from the $\ell = 2$ and $\ell = 3$ modes are $(6.8 \pm 0.4)\%M$ and 1.9% respectively, although boundary contamination is significant. Table II gives a summary of these results.

Figure 4 shows the track for the $+0.75$ configuration. Note that the spiral is much tighter than in the -0.75 configuration, and that the binary completes roughly 2.8 orbits before the common horizon forms. Note also that the first common horizon is much smaller

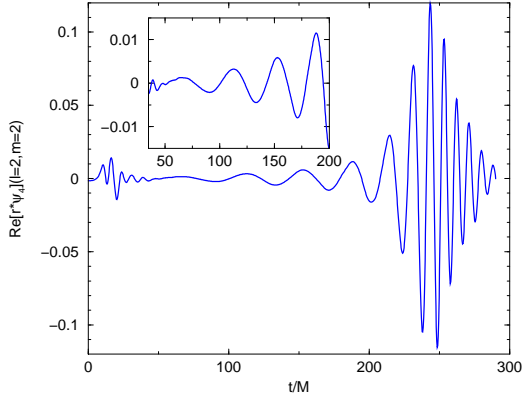


FIG. 3: The real part of the ($l=2; m=2$) mode of the r_4 in the Quasi-Kinnersley frame at $r=10M$ from the $+0.75'$ configuration. The inset shows a magnified view of the early orbital motion. Note that the $+0.75'$ waveform has 6 wavelengths of orbital motion prior to the plunge waveform (at $t=235M$), indicating that the binary orbited approximately three times before merging.

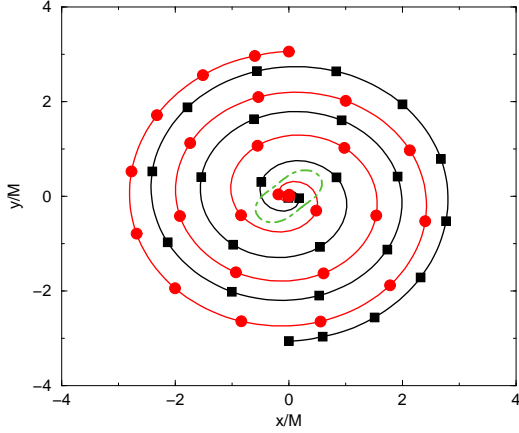


FIG. 4: The puncture trajectories on the xy plane for $+0.75'$ configuration with resolution $M=30$. The spirals are the puncture trajectories with ticks every $10M$ of evolution. The dot-dash 'peanut shaped' figure is the first detected common horizon at $t=224.5M$. The period of the last orbit is around $36M$. The last orbit begins when the punctures are located at $1.4M$ from the origin (in these coordinates).

in this case (in these coordinates) than in the $-0.75'$ case.

To demonstrate consistency with the General Relativity field equations, we calculated the Hamiltonian constraint violation. The constraint converges to fourth-order outside a small region surrounding the puncture (the constraint violation on the nearest neighboring points to the puncture is roughly independent of resolution, but this non-converging error does not propagate outside the individual horizons). Figure 5 shows the Hamiltonian constraint violations for the $-0.75'$ configuration along the

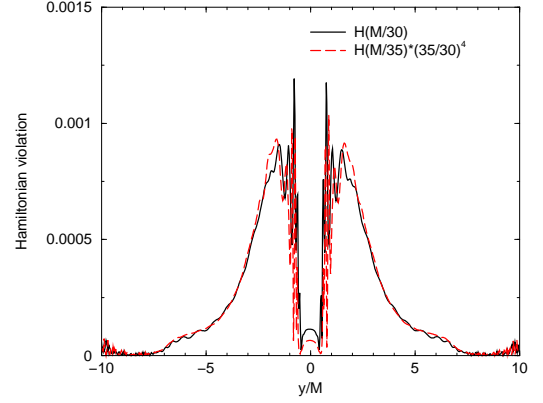


FIG. 5: The Hamiltonian constraint violation at $t=80M$ along the y -axis for the $M=30$ and $M=35$ runs (the latter rescaled by $(35/30)^4$) for the $-0.75'$ configuration. The punctures crossed the y -axis for the second time at $t=75M$. Note the reasonable fourth-order convergence. Points contaminated by boundary errors have been excluded from the plot. The high frequency violations near the numerical coordinate $y=M=9$ are due to the extreme sheyeresolution near the boundary, and converge with resolution.

TABLE II: Results of the evolution as determined from the waveform and the remnant horizon. The horizon formed at $t=224.5M$ for the $+0.75'$ configuration and $t=105.5M$ for the $-0.75'$ configuration. Estimates of the radiated angular momentum based on the waveform are less accurate due to truncated waveforms (in the $-0.75'$ case), and boundary contamination (in the $+0.75'$ case).

$S=m^2$	$E_{\text{rad}}=M_{\text{ADM}}$	$J_{\text{rad}}=J_{\text{ADM}}$	$a=M_H$	Method
$+0.75$	(6.0 1)%	(32.5 1.5)%	0.899 0.002	Horizon
$+0.75$	(6.8 1)%			Waveform
-0.75	(2.1 0.1)%	(26 2)%	0.44 0.01	Horizon
-0.75	(2.1 0.2)%			Waveform

y -axis at $t=80M$ (approximately $5M$ after the punctures cross the y -axis for the second time) for the $M=30$ and $M=35$ runs. The constraint is convergent everywhere except points contaminated by boundary errors (these points have been removed from the plot).

V. DISCUSSION

In this paper we have shown that the 'moving puncture' approach can be used to accurately simulate the inspiral orbit of spinning-black-hole binaries. We have found that the merger temporarily stalls when the total angular momentum (orbital plus spin) is larger than unity (in units of M^2). These binaries undergo several additional orbits (compared to spinless binaries), until the excess angular momentum is radiated away. The black holes then merge to form a single Kerr black hole with rotation parameter $a/M < 1$.

A linear fitting of our results, as well as those from the spinless case [11], leads to the simple extrapolation formula $a = M(0.68 + 0.3(S - m^2))$. Although more accurate simulations are needed, these results show that it is very unlikely to form a nearly maximally rotating black hole out of the merger of two highly spinning ones. Our results reinforce the same qualitative conclusions reached with the Lazarus approach [21].

For the $\chi = 0.75$ case the last orbit lasts 120M starting at a separation of 7M in coordinate space, while for the $\chi = 0.75$ case we have found that the duration of the last orbit is 36M at a coordinate separation of 2.8M. It is worth noting from [20], that the orbital period associated with the ISCO for the $\chi = 0.17$ case is roughly 27M at a coordinate separation of 1.6M, and that no ISCO was found for higher spin configurations. This highlights again the importance of the gravitational radiation in the late binary black hole dynamics which is not captured in the determinations of the ISCO. On the other hand, the dependence of the ISCO on spin correctly implies that the $\chi + \chi'$ configurations are more stable at close separations than the $\chi - \chi'$ configurations. This stability is seen in the significantly tighter spiral observed in Fig. 4.

Many outstanding issues involving spinning black hole scenarios remain to be explored. We plan to study some

of them next, including additional values of the individual spins for the $\chi + \chi'$ cases in order to better extrapolate the results to the limiting maximally rotating individual holes, as well as unaligned spins to, for instance, reproduce the change in the spin orientation suggested by the X-shaped radio lobes in active galactic nuclei [1]. Finally, more significant computer resources and the use of Adaptive Mesh Refinement techniques combined with higher order finite difference methods will be needed to achieve the accuracy required to aid gravitational wave detection efforts [34].

Acknowledgments

We thank Bernard Kelly for careful reading of this text. We thank Erik Schnetter for providing the Cactus thorns to implement P_i-symmetry boundary conditions. We gratefully acknowledge the support of the NASA Center for Gravitational Wave Astronomy at University of Texas at Brownsville (NAG 5-13396) and the NSF for financial support from grants PHY-0140326 and PHY-0354867. Computational resources were performed by the 64-node Funes' cluster at UTB.

-
- [1] D. Merritt and R. D. Ekers, *Science* 297, 1310 (2002), astro-ph/0208001.
 - [2] R. Shafee et al., *Astrophys. J.* 636, L113 (2006), astro-ph/0508302.
 - [3] S. L. Shapiro, *Astrophys. J.* 620, 59 (2005), astro-ph/0411156.
 - [4] C. F. Gammie, S. L. Shapiro, and J. C. McKinney, *Astrophys. J.* 602, 312 (2004), astro-ph/0310886.
 - [5] M. Volonteri, P. Madau, E. Quataert, and M. J. Rees, *Astrophys. J.* 620, 69 (2005), astro-ph/0410342.
 - [6] B. Brügmann, W. Tichy, and N. Jansen, *Phys. Rev. Lett.* 92, 211101 (2004), gr-qc/0312112.
 - [7] P. Diener et al., *Phys. Rev. Lett.* 96, 121101 (2006), gr-qc/0512108.
 - [8] F. Pretorius, *Phys. Rev. Lett.* 95, 121101 (2005), gr-qc/0507014.
 - [9] M. Campanelli, C. O. Lousto, P. Marronetti, and Y. Zlochower, *Phys. Rev. Lett.* 96, 111101 (2006), gr-qc/0511048.
 - [10] J. G. Baker, J. Centrella, D.-I. Choi, M. Koppitz, and J. van Meter, *Phys. Rev. Lett.* 96, 111102 (2006), gr-qc/0511103.
 - [11] M. Campanelli, C. O. Lousto, and Y. Zlochower, *Phys. Rev. D* 73, 061501(R) (2006).
 - [12] J. G. Baker, J. Centrella, D.-I. Choi, M. Koppitz, and J. van Meter (2006), gr-qc/0602026.
 - [13] F. Pretorius (2006), gr-qc/0602115.
 - [14] M. Campanelli, *Class. Quant. Grav.* 22, S387 (2005), astro-ph/0411744.
 - [15] F. Herrmann, D. Shoemaker, and P. Laguna (2006), gr-qc/0601026.
 - [16] J. G. Baker et al. (2006), astro-ph/0603204.
 - [17] J. Baker, M. Campanelli, C. O. Lousto, and R. Takahashi, *Phys. Rev. D* 65, 124012 (2002), astro-ph/0202469.
 - [18] J. M. Bowen, *Gen. Rel. Grav.* 11, 227 (1979).
 - [19] S. Brandt and B. Brügmann, *Phys. Rev. Lett.* 78, 3606 (1997), gr-qc/9703066.
 - [20] H. Pfeiffer, S. A. Teukolsky, and G. B. Cook, *Phys. Rev. D* 62, 104018 (2000), gr-qc/0006084.
 - [21] J. Baker, M. Campanelli, C. O. Lousto, and R. Takahashi, *Phys. Rev. D* 69, 027505 (2004).
 - [22] cactusweb, cactus Computational Toolkit home page: <http://www.cactuscode.org>.
 - [23] R. M. Wald, *General Relativity* (The University of Chicago Press, Chicago, 1984), ISBN 0-226-87032-4 (hardcover), 0-226-87033-2 (paperback).
 - [24] L. E. Kidder, *Phys. Rev. D* 52, 821 (1995), gr-qc/9506022.
 - [25] L. Blanchet, *Pramana* 53, 1 (1999), gr-qc/0403122.
 - [26] S. Dain, C. O. Lousto, and R. Takahashi, *Phys. Rev. D* 65, 104038 (2002), gr-qc/0201062.
 - [27] Y. Zlochower, J. G. Baker, M. Campanelli, and C. O. Lousto, *Phys. Rev. D* 72, 024021 (2005), gr-qc/0505055.
 - [28] T. Nakamura, K. Oohara, and Y. Kojima, *Prog. Theor. Phys. Suppl.* 90, 1 (1987).
 - [29] M. Shibata and T. Nakamura, *Phys. Rev. D* 52, 5428 (1995).
 - [30] T. W. Baumgarte and S. L. Shapiro, *Phys. Rev. D* 59, 024007 (1999), gr-qc/9810065.
 - [31] M. A. Kubiś, B. Brügmann, P. Diener, M. Koppitz, D. Pollney, E. Seidel, and R. Takahashi, *Phys. Rev. D* 67, 084023 (2003), gr-qc/0206072.
 - [32] M. Campanelli, B. Kelly, and C. O. Lousto, *Phys. Rev.*

- D 73, 064005 (2005), gr-qc/0510122.
- [33] J. Thomburg, *Class. Quantum Grav.* 21, 743 (2004), gr-qc/0306056.
- [34] M. Miller, *Phys. Rev. D* 71, 104016 (2005), gr-qc/0502087.
-